Time-resolved spontaneous Raman spectroscopy of infrared-multiphoton-excited SF_6

Jyhpyng Wang, Kuei-Hsien Chen, and Eric Mazur
Department of Physics and Division of Applied Sciences, Harvard University, Cambridge, Massachusetts 02138
(Received 22 May 1986)

Spontaneous Raman spectroscopy is used as a tool for studying the vibrational energy distribution of collisionless infrared-multiphoton-excited SF_6. A collisionless increase in Stokes and anti-Stokes signals from the strong Raman-active ν_1 mode is observed after infrared-multiphoton excitation by a high-power 500-ps CO_2-laser pulse tuned to the infrared active ν_3 mode. Results are presented over a pressure range from 13 Pa (100 mTorr) to 270 Pa (2 Torr). The pressure dependence clearly proves that the increase does not depend on collisions. The effects are studied as a function of time and of the infrared energy fluence, infrared wavelength, and infrared pulse duration. The experimental data show that an intramolecular equilibrium of vibrational energy is established within the 20-ns time resolution of the experimental setup. The multiphoton excitation shows a red shift and intensity broadening. A comparison with results from photoacoustic measurements is made.

I. INTRODUCTION

In 1973 it was discovered that isolated molecules in the ground electronic state can be dissociated by a short, intense pulse from a CO_2-laser.[1] During the last decade the absorption of many monochromatic infrared photons by isolated molecules, called infrared multiphoton excitation, has been studied extensively by many groups.[2] It was found that this is a general property of polyatomic molecules that have an infrared active mode resonant with the laser field. The dependence of multiphoton excitation on infrared intensity, fluence, frequency and molecular size, as well as spectra of infrared multiphoton excited molecules have been reported. Technological applications of infrared multiphoton excitation have also been developed: Examples are isotope separation,[3–6] unimolecular reactions,[7,8] and molecular synthesis.[9] At the same time several theoretical approaches have been proposed to describe this phenomenon.[10–15] Because the spectrum of vibrational and rotational transitions between excited vibrational states is not well known, multiphoton excitation has proven difficult to describe quantitatively. Although most of the conceptual ideas of the theory have been verified experimentally, many open questions remain.

One question that has been receiving recent attention concerns the intramolecular distribution of energy in infrared multiphoton excited molecules.[16] As is well-known, collisions with other molecules rapidly equilibrate vibrational energy among the different molecular degrees of freedom. In the absence of collisions, however, the energy distribution mechanisms in highly vibrationally excited molecules are not yet well understood. At high excitation the spacing between vibrational levels becomes increasingly smaller and many quasi-isoenergetic combinations of states exist. In this regime molecular excitation occurs mostly through incoherent one-photon transitions between states that are defined by total energy content. Since the number of states involved is large — and often not even known — the problem is inherently complicated, even for a modest size molecule. Moreover, the lack of spectroscopic data of highly excited states renders a complete quantum mechanical treatment of the excitation dynamics nearly impossible. So it is in general not possible to determine the intramolecular distribution of energy in infrared multiphoton excited molecules *a priori*.

A statistical description of the ensemble of modes within a single molecule has therefore been proposed as an alternative.[17,18] Nonlinear dynamics studies have shown that energy can swing back and forth between two coupled oscillators in such a way that — in the sense of a time-average — energy is equipartitioned.[19] This conclusion agrees with recent experiments,[20] where transfer of energy between two closely spaced, isolated, modes has been demonstrated by observing the beating fluorescence signal from these modes. For a system consisting of many coupled oscillators, such as a highly vibrationally excited polyatomic molecule, there are many channels for transferring excitation energy. Since the period of Poincaré cycles is an exponential function of the dimension of phase space,[21] it exceeds the mean free time between collisions even for a modest size molecule at pressures above 10 Pa. Therefore intramolecular vibrational energy transfer in a highly excited polyatomic molecule can be considered irreversible for all practical purposes. A statistical description implies an intramolecular equilibrium distribution of energy among the various modes of an infrared multiphoton excited molecule on collisionless time scales. The aim of our present research effort is to establish experimentally whether such an approach is justified.

Direct experimental information on both intramolecular and intermolecular energy distribution after infrared multiphoton excitation has been obtained by spontaneous Raman spectroscopy[22–27] and from infrared double resonance experiments.[28–30] In this paper we elaborate on a previously reported experiment,[31] in which internal energy leakage from an infrared active mode to a Raman active mode is observed by monitoring the evolution of the anti-Stokes Raman

signal. Both collisional and collisionless aspects will be discussed.

II. THEORY

In this section we present a brief treatment of spontaneous Raman scattering, in order to derive a simple expression for the total intensity of the light scattered from a Raman active mode. Both radiation field and molecular system are treated quantum mechanically. To describe the mechanism of Raman scattering we consider the interaction of the field with the induced polarization P of the molecule,

$$P = \mu_0 + \alpha \cdot E, \tag{1}$$

where μ_0 is the permanent dipole moment of the molecule, α a tensor representing the molecular polarizability, and $\alpha \cdot E$ the induced dipole moment. The physical system is described by the Hamiltonian operator, which contains terms describing the molecular system and the electromagnetic radiation field, and a term representing the interaction between the molecular polarization and the field. This last term, the interaction Hamiltonian H_{int}, is responsible for the light scattering. In the electric-dipole approximation one has

$$H_{\text{int}} = E \cdot \alpha \cdot E \, . \tag{2}$$

Following Placzek[32] one expands the molecular polarizability α as a Taylor series of the generalized coordinate q of the molecular vibrational mode being considered

$$\alpha = \alpha_0 + \left(\frac{\partial \alpha}{\partial q}\right)_0 q + \frac{1}{2}\left(\frac{\partial^2 \alpha}{\partial q^2}\right)_0 q^2 + \ldots \, . \tag{3}$$

Substituting α into H_{int} we obtain,

$$H_{\text{int}} = E \cdot \alpha \cdot E + E \cdot \left(\frac{\partial \alpha}{\partial q}\right)_0 \cdot E\, q + \frac{1}{2} E \cdot \left(\frac{\partial^2 \alpha}{\partial q^2}\right)_0 \cdot E\, q^2 + \ldots \, . \tag{4}$$

The first term represents the Rayleigh scattering, the remaining terms first and higher order Raman scattering. Since higher order scattering is rejected in our experiment, we need only consider the term linear in q. In simple harmonic approximation we have

$$q = (h/8\pi^2 \mu \nu_R)^{1/2} [\, b^\dagger + b \,] \tag{5}$$

where $b^\dagger$ and b are the creation and annihilation operator for the vibrational quanta respectively, and ν_R the frequency of the harmonic oscillator. The field is quantized similarly:

$$E_\lambda = (2\pi h \nu_R/\varepsilon V)^{1/2} \sum \mathbf{e}_\lambda \, i \, [\, a_\lambda^\dagger - a_\lambda \,] \tag{6}$$

with $a^\dagger$ and a the creation and annihilation operators for the field, ε the relative permittivity, V the mode volume, and $\mathbf{e}_\lambda$ a unit vector representing the polarization of the light of wavelength λ. The linear term in the interaction Hamiltonian can therefore be written in the following form,

$$H_{\text{int}} \sim \left(\frac{\partial \alpha}{\partial q}\right)_0 \{ a_L b\, a_{AS}^\dagger + a_L b^\dagger a_S^\dagger \} (\mathbf{e}_L \cdot \mathbf{e}_R) \, , \tag{7}$$

where the indices L, AS, S and R stand for laser, anti-Stokes, Stokes and Raman respectively. The first term in this expression annihilates a vibrational quantum and therefore corresponds to the anti-Stokes branch. The second term corresponds to the Stokes branch. The transition probability from an initial state $| i \rangle$ to a final state $| f \rangle$, is given by

$$W_{i \to f} = |\langle f | H_{\text{int}} | i \rangle|^2 \, . \tag{8}$$

For the eigenstates $|n\rangle$ of the harmonic oscillator one has

$$b^\dagger | n \rangle = (n+1)^{1/2} | n+1 \rangle \, , \tag{9}$$

and

$$b | n \rangle = n^{1/2} | n-1 \rangle \, , \tag{10}$$

with n the vibrational quantum number corresponding to state $|n\rangle$.

From eqs. (7) through (10) it can now immediately be seen that the transition probabilities for Stokes and anti-Stokes transitions depend on $n+1$ and n, respectively

$$W_{n \to n+1} \sim n+1, \quad W_{n \to n-1} \sim n. \tag{11}$$

Hence the *total* intensity of the spontaneous Stokes and anti-Stokes Raman signals (summed over *all* vibrational levels of the particular vibrational mode considered), I_S and I_{AS}, are given by

$$I_S \sim \sum_{n=0}^{\infty} W_{n \to n+1} N(n) \sim \sum_{n=0}^{\infty} (n+1) N(n) = 1 + \sum_{n=1}^{\infty} n N(n) \, , \tag{12}$$

$$I_{AS} \sim \sum_{n=0}^{\infty} W_{n \to n-1} N(n) \sim \sum_{n=1}^{\infty} n N(n) \, ,$$

with $N(n)$ the population of level n. Substituting the average energy in the mode per molecule, $E_R = h\nu_R \sum n N(n)$, we find for the summations in eq. (12)

$$I_S \sim 1 + \frac{E_R}{h\nu_R} \, , \qquad I_{AS} \sim \frac{E_R}{h\nu_R} \, . \tag{13}$$

It is important to note that in the harmonic approximation the result obtained does not depend on the energy distribution $N(n)$, but only on the *average* energy E_R.

Thus, the intensity of a Raman active mode is a measure for the average energy content of the mode. This can then be compared with the energy content of other modes and with the total energy deposited into the sample. Such a comparison will tell how the absorbed energy is distributed in the absence of collisions.

III. EXPERIMENTAL METHOD AND APPARATUS

A schematic view of the setup is shown in Fig. 1. An infrared exciting beam and an ultraviolet probing beam cross inside a scattering cell[33]. The spontaneous Raman signal of the SF_6 molecules is detected along the direction perpendicular to the incident beams. The scattering cell consists of two orthogonal arms, that contain a series of black anodized baffles, arranged to trap scattered or diffracted light, see Fig. 2. Light scattered in the interaction region is collected over a solid angle of $\pi/16$ sr, and focused onto the entrance slit of a double monochromator of 3 nm resolution. The output from the monochromator is detected by a fast ultraviolet-sensitive photomultiplier. Since the number of photons that reach the photomultiplier per laser pulse is less than ten, the signal has to be averaged over a large number of shots, typically 10^4.

The short-pulse CO_2-oscillator-amplifier system is shown in Fig. 3. The laser pulse originates in the 241 cm

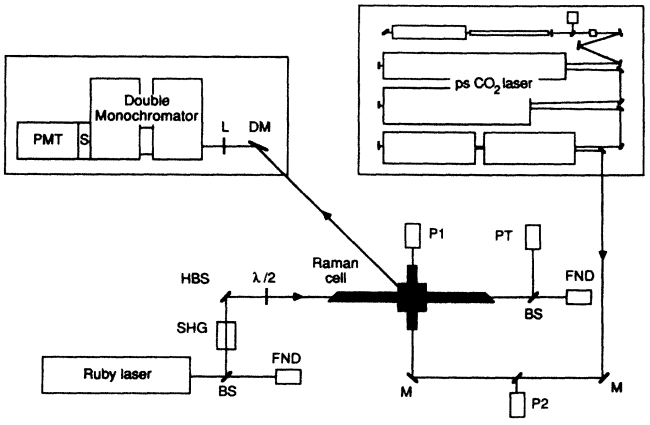

FIG. 1. Setup for measuring the spontaneous Raman scattering from infrared multiphoton excited molecules at low densities. Molecules excited by a CO_2-laser are probed by the second harmonic of a Ruby laser. BS = beam splitter, SHG = second harmonic generator, HBS = harmonic beam splitter, $\lambda/2$ = half-wave plate, FND = fast photodiode, PT = photo-tube, P1, P2 = pyroelectric detector, M = mirror, DM = dichroic mirror, L = quartz lens, S = shutter, PMT = photomultiplier tube. The detection (monochromator, photomultiplier, etc.) is located in a light-tight enclosure located directly above the Raman cell. Drawing not to scale.

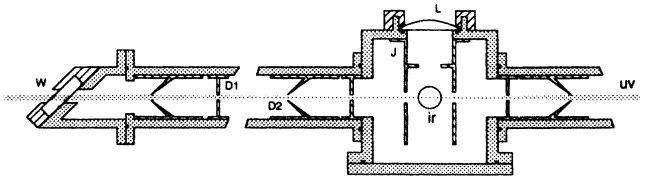

FIG. 2. Cross-sectional view of the Raman cell. W = quartz window, D1, D2 = straight and conical baffles, J = stray light jacket, IR = position of ir pump beam, UV = probing uv beam, L = collimating lens. The window holder has been rotated by 90° to show the Brewster angle mounting.

long cavity of a hybrid CO_2-laser, with a 62 MHz longitudinal mode spacing. The cavity consists of a transversely excited atmospheric-pressure (TEA) section and a low pressure (500 Pa) continuous wave (CW) discharge cell. Since the TEA section, a Taschisto Model 215 CO_2-laser head, has a bandwidth of 3.6 GHz, the laser can oscillate on many modes simultaneously. The low pressure section, which has a 55 MHz bandwidth, however, acts as an active filter and allows only one longitudinal mode in the cavity.[34] To prevent the laser from occasionally lasing on two adjacent modes, each laser pulse is monitored by a fast detector. When lasing on two modes occurs, the detector signal has a beat frequency of 62 MHz. An electronic circuit then adjusts the length of the laser cavity with a piezoelectric transducer to restore single mode operation.

The single mode output pulses from this hybrid laser, which have a 100 ns full-width at half maximum duration, are truncated by a self-triggered plasma shutter.[35,36] The truncated pulses have a slow rise time — identical to the rise time of the 100 ns pulses — and an ultra-short fall time of about 10 ps. The pulses are further shortened by optical free induction decay (OFID) in a 4 m long low-pressure CO_2-cell.[37] The output pulse duration can be varied continuously from 30 to 250 ps by adjusting the pressure in the cell from 30 kPa to 4 kPa. The peak power of the short pulse

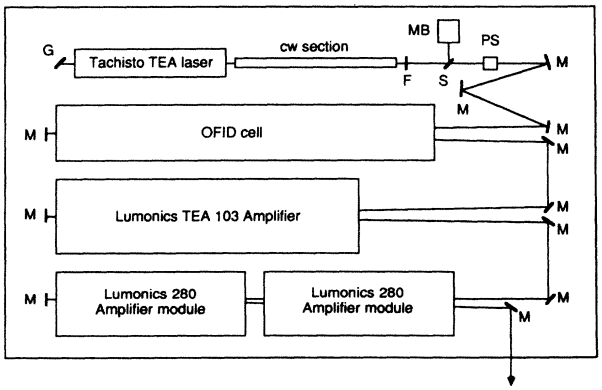

FIG. 3. The short-pulse CO_2-oscillator-amplifier system used for the infrared multiphoton excitation of the SF_6 (see text for explanation). G = grating, F = output coupler, S = beam splitter, MB = mode-beat detector, PS = plasma shutter, M = mirror.

generated is equal to that of the input pulse, while the total energy is decreased by a factor that is the ratio of the duration of output and input pulses.

One Lumonics model 103 laser amplifier operating at atmospheric pressure and two 10 atm Lumonics model 280 amplifiers are used to boost the energy of the short laser pulse. The atmospheric pressure amplifier, which has the smallest bandwidth, limits the pulse duration to 500 ps. With the high pressure amplifiers, which have a much larger bandwidth, pulses shorter than 50 ps can be amplified without significant stretching. The output beam is focused into the scattering cell by a cylindrical lens. Depending on the optical arrangement used, the beam waist is 2.2×0.18 mm or 6×0.35 mm. The average output energy is 100 mJ.

The probe beam is generated by a Raytheon model SS-420 Q-switched ruby laser that is frequency-doubled with a RDA-crystal second harmonic generator. The second harmonic at 347.15 nm is vertically polarized, i.e. in the direction of detection. A half-wave plate rotates the polarization by 90° into the plane of the two laser beams to obtain a maximum cross-section for Raman scattering, see Eq. (7). The beam is focused into the scattering region, where it crosses the infrared laser beam. The beam waist at the focal point is 500 mm, and the average probing pulse energy is 5 mJ.

A 0.3 Hz pulse generator controls the timing of the lasers and the data-acquisition system. The trigger pulses are optically isolated to prevent feedback of radio-frequency noise from the lasers. The synchronization of lasers and amplifiers is controlled electronically. The accuracy is limited by the 100 ns jitter of the lasers. Since this is inadequate for our measurements, the time-delay between infrared and ultraviolet pulses is measured for each pair of pulses. Two fast detectors provide start and stop pulses for an EG&G model 457 time to pulse-height converter, which measures the time delay between the two laser pulses. Although the resolution of the time to pulse-height converter is better than 100 ps, the time resolution of the setup is limited by the 18 ns duration of the probe beam, which we plan to improve in the near future. The energy of pump and probe pulses are measured by a pyroelectric detector and a phototube, respectively. Two electrodes, placed around the focal point of the plasma shutter, allow monitoring of the plasma breakdown. A small electronic circuit can thus determine if the infrared pulses are truncated correctly. All signals are collected by a data-acquisition system that is controlled by a Digital PRO 350 microcomputer.

The 19-channel data-acquisition system is shown in Fig. 4. It consists of home-made pulse sampling electronics, and a computer automated measurement and control (CAMAC) crate, containing a multiplexer, analog-to-digital converter, general input/output interface, and a general purpose interface bus (GPIB) crate controller. For every laser pulse, the pulse generator provides two trigger pulses to the data-acquisition system, one 100 ms before and one immediately after the lasers fire. This makes it possible to correct for a baseline-offset each time the signals are sampled. All data from the sample and hold circuits are converted to digital signals by the multiplexer and analog-to-digital converter. To correct for dark counts, the photomultiplier tube signal is recorded by a Biomation model 8100 transient waveform digitizer with 10 ns sampling intervals. The crate controller provides the interface to the computer, which in addition to reading and storing data, also monitors the values and rejects invalid data. A more detailed description of the experimental setup can be found in Ref. 33.

For the measurements presented in this paper, the following signals were recorded: Raman signal intensity, input energy and time-delay of ultraviolet and infrared pulses, ruby laser energy, and plasma breakdown. For every measurement the various signals are calibrated. The pyroelectric detector, which monitors the infrared pumping energy, is calibrated with a Scientech Joule meter, and the ultraviolet phototube, which monitors the ultraviolet probing pulse energy, with a Molectron pyroelectric detector. The photomultiplier signal is calibrated by measuring the room temperature Stokes sig-

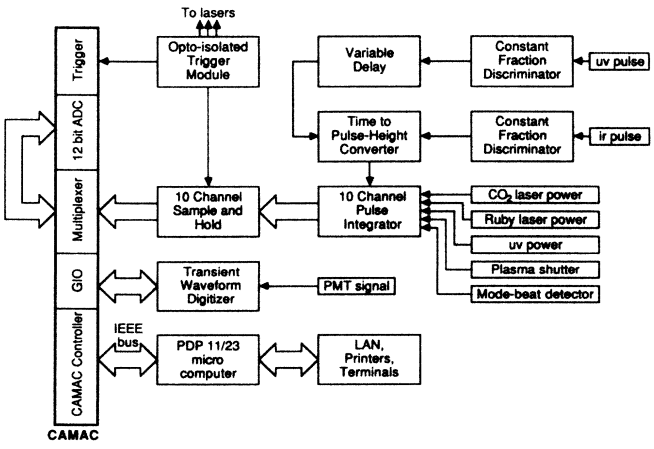

FIG. 4. Schematic diagram of the multichannel data-acquisition system.

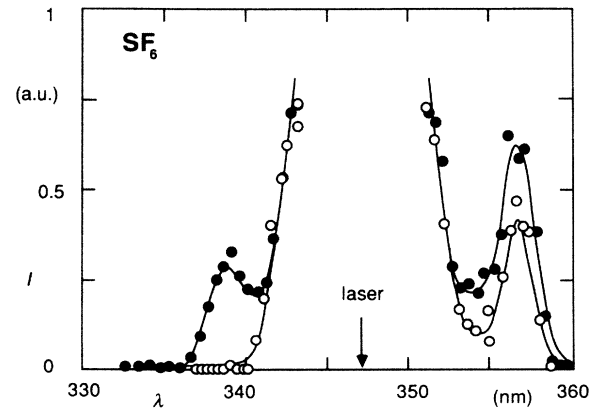

FIG. 5. Raman spectrum of SF_6, with (closed symbols) and without (open symbols) infrared multiphoton excitation. Infrared excitation: 10.6 μm P(20) line, 0.5 ns pulse duration, and average fluence 0.6×10^4 J/m^2. The small arrow shows the position of the laser radiation at 347.15 nm.

nal without infrared multiphoton excitation, henceforth referred to as 'thermal Stokes,' as a reference.

As we are dealing with small signals, several consistency checks were performed to ensure that no systematic errors occur. It was verified that there are no signals without ultraviolet probing pulse, or without gas in the scattering cell, and no anti-Stokes signal for negative time-delay. Reproducibility of the measurements was checked routinely during each measurement and from measurement to measurement.

Data analysis starts with a histogram of the infrared energy values. Then, the datapoints within the optimal range of infrared energy are further analyzed. The data are further restricted to include only valid data and subsequently calibrated and plotted. All Raman signals are normalized with the ultraviolet pumping intensity and the thermal Stokes signal so that the results from different measurements can be compared. Each individual measurement carried out at a fixed pressure contains enough datapoints to obtain the time and fluence dependence of the Raman signals. The pressure dependence was obtained separately by varying the pressure within one experimental run.

IV. RESULTS

Experiments have been performed at room temperature on SF_6 at sample pressures ranging from 13 Pa to 270 Pa. The SF_6 gas, obtained commercially, had a purity of 99.995%. Data were obtained for the CO_2-laser frequencies between the P(12) and P(28) lines of the 10.6 μm branch, which are resonant with the triply degenerate infrared active ν_3-mode (F_{1u}) of SF_6. Two different pulse durations were employed: short 0.5 ns and truncated 15 ns full-width at half-maximum pulses with fluences up to 7×10^4 J/m^2. The 15 ns truncated pulses are obtained with an optical free induction decay cell pressure of 1.3 kPa. At these low pressures, the pulses have an asymmetric shape, with a 10-90% rise time of 10 ns and a short subnanosecond fall time. The Raman signals are obtained at a shift of 775 cm^{-1} from the frequency-doubled ruby laser, corresponding to the totally symmetric breathing ν_1-mode (A_{1g}) of SF_6. Results are shown in Figs. 5 through 12. The vibrational modes of SF_6 are given in Table I.[38]

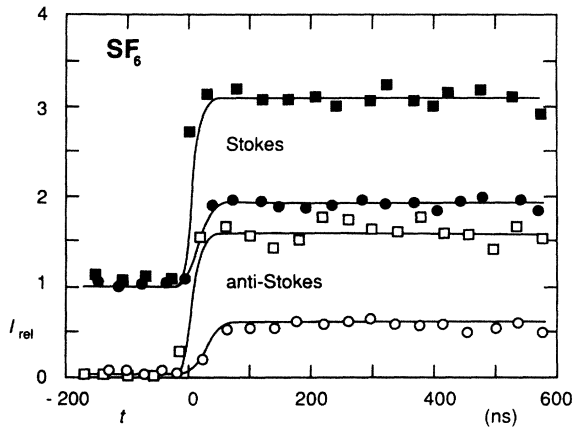

FIG. 6. Intensity of Stokes (closed symbols) and anti-Stokes (open symbols) signal as a function of the time delay between pump and probe pulses at a pressure of 67 Pa. The data are normalized to the thermal Stokes signal. Negative time delay means that the signals are measured before the infrared multiphoton excitation. The rise time in the curves reflects the 18 ns FWHM duration of the probe pulse. Results are shown for two different durations, 0.5 ns (squares) and 15 ns (circles). Infrared excitation at the 10.6 μm P(20) line, with an average fluence of 0.8×10^4 J/m^2.

The points shown in the figures are obtained by dividing the x-axis into a number of intervals (usually twenty), and averaging the data that lie within each of the intervals. Since our experiment is done in the photon counting regime, the standard deviation of the photomultiplier signal is comparable to its average value, even when the data is restricted to those data points where the fluctuation in the pump laser intensity is no more than 20%. According to the central limit theorem, the standard deviation in average value for a certain interval is inversely proportional to the square root of the number of data within that interval.[39] Typically, at 100 Pa, about 200 laser pulses are needed to obtain a 10% standard deviation. Since the experiment is carried out at a repetition rate of 0.3 Hz, the stability of the alignment limits the total number of shots to 10^4 for a single experimental run. This means that there is a trade-off between the number of points in one figure and

TABLE I. Vibrational modes of SF_6, taken from Ref. 38 (s = strong, w = weak).

Mode	k (cm^{-1})	ν (THz)	symmetry	degeneracy	activity
ν_1	775	23.25	A_{1g}	1	Raman (s)
ν_2	644	19.32	E_g	2	Raman (w)
ν_3	965	28.95	F_{1u}	3	infrared
ν_4	617	18.51	F_{1u}	3	infrared
ν_5	524	15.72	F_{2g}	3	Raman (w)
ν_6	363	10.89	F_{2u}	3	inactive

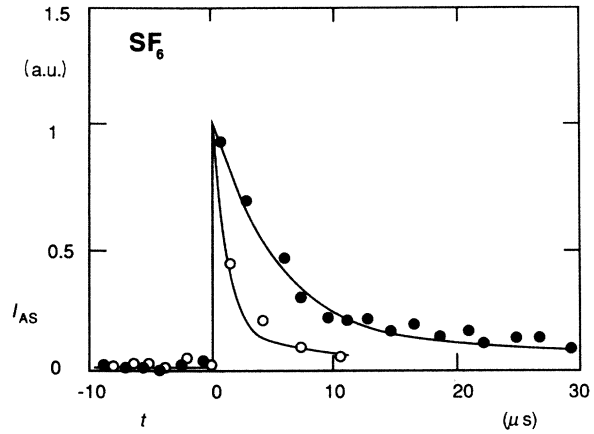

FIG. 7. Long time behavior of the anti-Stokes signal for two pressures: p = 70 Pa (open symbols) and p = 270 Pa (closed symbols). The signal is normalized to one at $t = 20$ ns. Infrared excitation: 10.6 μm P(20) line, 0.5 ns pulse duration, and average fluence 10^4 J/m^2. The decay of the curves, which is due to diffusion of the excited molecules out of the interaction region, scales with pressure (see text for details).

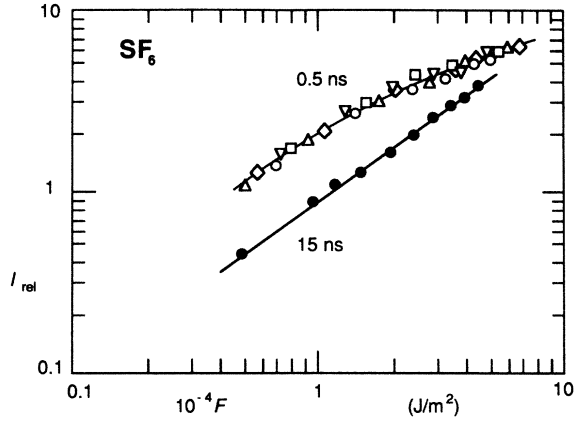

FIG. 9. Relative anti-Stokes signal as a function of the infrared pumping fluence for various pressures and two infrared pulse durations at the 10.6 μm P(20) line: 0.5 ns (open symbols) and 15 ns (closed symbols). This graph shows the reproducibility of the data from measurement to measurement.
□: 33 Pa; ○: 67 Pa; △ : 133 Pa;▽ : 200 Pa;
◇: 267 Pa; ●: 133 Pa.

the length of the error bars. In all measurements presented here the error bars are about 10% of the absolute value of the data points.

Fig. 5 shows the Raman spectrum of SF_6 with and without infrared pumping. The central peak is due to elastically scattered light — mainly Rayleigh scattering. The spectral resolution, which is determined by the slit of the monochromator, is 3 nm. Without the infrared pumping only a Stokes shifted peak is observed. This is because at room temperature less than 3% of the molecules are in excited states of the Raman active mode. With infrared pumping it is seen that both Stokes and anti-Stokes signals increase. Since the ν_3 and ν_1 modes have opposite symmetry, they do not couple at low excitation. This figure, however, clearly shows that under infrared multiphoton excitation the energy distribution of the Raman active mode is changed. It also shows that there is no contribution from elastically scattered light at the position of the Raman lines. The remainder of the experimental results are obtained at fixed frequencies, 356.7 nm and 338 nm for the Stokes and anti-Stokes lines, respectively.

Fig. 6 shows the increase of both Stokes and anti-Stokes signals as a function of the time delay between the infrared pump and the probe pulse for two infrared pulse durations, 0.5 ns and 15 ns at a pressure of 67 Pa and an average infrared fluence of 0.8×10^4 J/m^2. Negative time delay, $t < 0$, means that the molecules are probed before the

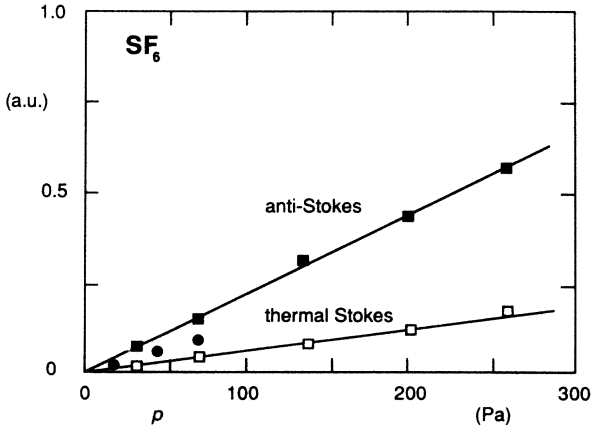

Fig. 8. Pressure dependence of anti-Stokes (closed symbols) and thermal Stokes (open symbols) signal. Infrared excitation for anti-Stokes data: 10.6 μm P(20) line, 0.5 ns (squares) and 15 ns (circles) pulse duration, and average fluence 2×10^4 J/m^2.

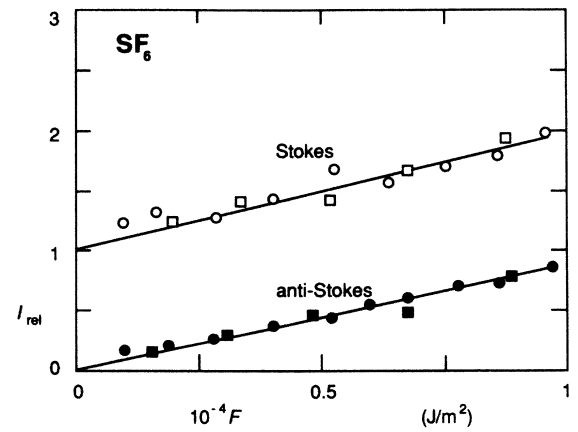

FIG. 10. Relative Stokes (open symbols) and anti-Stokes (closed symbols) signal as a function of the infrared pumping fluence at the 10.6 μm P(20) line for 15 ns pulses at two different pressures: $p = 27$ Pa (squares), and $p = 133$ Pa (circles).

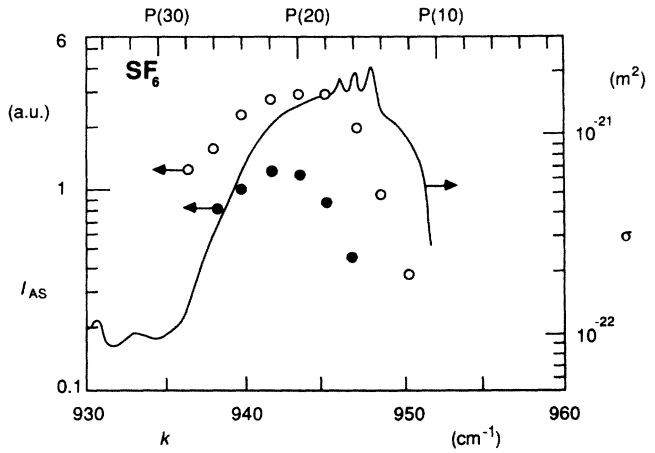

FIG. 11. Anti-Stokes signal for excitations at different CO_2-lines. The curve shows the one photon absorption cross section (see scale on the right). A clear red-shift can be observed. Data for two different pulse durations at an average fluence of 10^4 J/m^2 are shown: 0.5 ns (open symbols) and 15 ns (closed symbols). The position of the data points with respect to the right hand vertical scale is arbitrary.

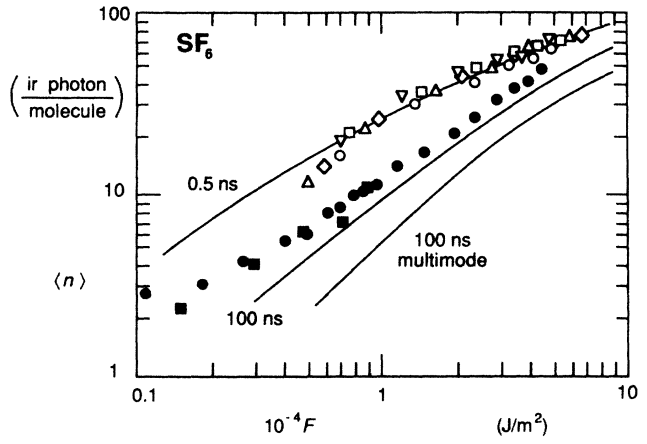

FIG. 12. Average number of infrared photons absorbed per molecule as a function of infrared fluence. The data points shown were obtained from the ones shown in Figs. 9 and 10, assuming thermal equilibrium between all vibrational modes immediately after the infrared multiphoton excitation. See those figures for an explanation of the symbols. The solid lines are the average number of infrared photons obtained from the photoacoustic measurements reported in Ref. 43. The results show a remarkable agreement.

infrared multiphoton excitation, i.e. the molecules are at thermal room temperature equilibrium. The Raman signals are normalized with the equilibrium room temperature (thermal) Stokes signal. Within the 20 ns time resolution of the experiment, determined by the duration of the ultraviolet pulse, a *collisionless* (see discussion) increase of both Stokes and anti-Stokes signals is observed. The increase is consistent with the result obtained in Eq. (13), i.e. for each pulse duration both Stokes and anti-Stokes signal increase by the same amount. After the initial increase the signals remain constant, even on a time scale on which collisional vibrational energy relaxation starts to play a role (the vibrational relaxation time constant, $\tau_{V\text{-}V}$, is given by $p\tau_{V\text{-}V} \approx 70\,\mu$s Pa).[40] Clearly, collisions do not affect the total intensity of the anti-Stokes signal. This shows that intramolecular equilibrium is reached on a time scale shorter than the time resolution. Since the intensity of the signal is determined by the average energy in the mode only, intermolecular vibrational-vibrational energy transfer will not affect the Raman signals once intramolecular equilibrium is reached.

The long time evolution of the anti-Stokes signal, measured at two different gas pressures, 70 and 270 Pa is shown in Fig. 7. The observed decay in the signals is about ten times faster than the relaxation time reported for collisional transfer of vibrational energy to translational degrees of freedom ($p\tau_{V\text{-}T} \approx 16$ ms Pa).[41] Moreover, the low pressure signal decays faster than the high pressure signal, showing the decay is not caused by collisional energy relaxation, but by diffusion of the excited molecules out of the interaction region — a process inversely proportional to pressure. Indeed, data points obtained at the higher pressure can be made to overlap the low pressure points by scaling the horizontal axis with pressure (see curves in Fig. 7).

Fig. 8 shows the pressure dependence of the signal, obtained by varying the pressure in a single experimental run. Both the anti-Stokes signal from infrared multiphoton excited molecules as well as the thermal Stokes signal from unexcited molecules are shown. The points lie on straight lines, which account for the trivial dependence of the signals on particle density. This figure excludes the possibility that the observed changes in Raman signal are caused by a collisional process, in which case one would expect to see a p^2-dependence.

The infrared fluence dependence of the Stokes and anti-Stokes signal is shown in Figs. 9 and 10 for different pressures and pulse durations. The results shown were obtained in different runs, each one calibrated individually. The spread in data therefore shows the absolute accuracy and the reproducibility of the experimental data. Fig. 10 shows once again that both Stokes and anti-Stokes signals increase by the same amount, in agreement with Eq. (13).

Fig. 11 shows the anti-Stokes signal for excitations at different CO_2-lines. Each point shown represents a separate experimental run in which the anti-Stokes signal was measured at a particular laser line. From each of these measurements, carried out with two different pulse durations, the infrared fluence dependence was obtained, yielding graphs similar to Fig. 10. One point from each of these fluence dependencies (at a fluence of 10^4 J/m^2) is shown here. As a reference the low signal absorption cross-section for SF_6 is also plotted.[42] The relation between the two vertical scales is arbitrary. Because of the anharmonicity of the mode the energy level spacing decreases with increasing excitation. Therefore a red shift from the center of the one photon absorption band is observed. Because of the low spectral resolution of 3 nm (250 cm^{-1}) of the present setup, a previously reported red shift of the Raman displacement,[25] could not be observed.

V. DISCUSSION

Within the 20 ns time-resolution of the experiment, an instantaneous collisionless increase of the anti-Stokes signal or, alternatively, the average energy stored in the Raman-active mode, is observed. If the energy distribution among the different vibrational modes is not in equilibrium, collisions would alter the energy in the Raman active mode, and consequently change the Raman signal intensity. Since the Raman signals remain constant (within the 10% experimental accuracy) for 1 μs after infrared multiphoton excitation, an intramolecular vibrational energy equilibrium must be established within the time-resolution of the experiment.

Further evidence of an intramolecular equilibrium is obtained by comparing the present results with the results obtained from photoacoustic measurements.[43] Since the Raman signals are proportional to the energy stored in the Raman active mode, the energy can be obtained from the relative increase in anti-Stokes signal

$$E_R = h\nu_R \, I_{rel} / [1 - \exp(-h\nu_R / kT_0)], \tag{14}$$

where I_{rel} is the ratio between the anti-Stokes signal and the thermal Stokes signal, k the Boltzmann factor, and T_0 room temperature. This equation is obtained from Eq. (13) and the Boltzmann value of the energy in the mode at room temperature. If one assumes intramolecular equilibrium among the different vibrational modes, the energy distribution of the different modes should correspond to a common temperature. The total increase in vibrational energy of the molecule can thus be calculated from this temperature, and compared to the total absorbed energy, obtained from the photoacoustic measurements. The result of this comparison is shown in Fig. 12. The average total energy absorbed per molecule in units of pumping infrared photons is plotted as a function of infrared fluence. The data points are obtained from the current experiments, while the curves show the results of the photoacoustic measurements from Ref. 43. The agreement between the two measurements is remarkable, providing strong evidence for an intramolecular equilibrium.

It should be pointed out that the photoacoustic measurements monitor all molecules absorbing one or more infrared photons, while the Raman measurements only involve the fraction of molecules absorbing enough photons to reach the region where the infrared and Raman active mode couple to each other, a region frequently referred to as the quasicontinuum.[17] Consequently the curve for the Raman experiment should fall off more rapidly for low fluences than the one for the photoacoustic experiment, since the fraction of excited molecules is smaller. This is indeed observed for fluences below 10^4 J/m^2.

Another remarkable feature is that a collisionless increase in anti-Stokes signal within 20 ns can still be observed at infrared fluences as low as 3×10^2 J/m^2,[31] where the average infrared absorption of SF_6 is reported to be below 1 photon per molecule.[43] At these fluences the *inter*molecular vibrational energy distribution — in contrast to the *intra*molecular distribution — is not in equilibrium: Apparently even at low infrared fluence a small yet measurable fraction of molecules is excited high enough to show a change in Raman spectrum, while most molecules remain unexcited. Such a bimodal distribution, consisting of some highly excited molecules and the others unexcited, is consistent with a recent observation of two or three photon transitions in a pulse jet of SF_6 at infrared fluences below 2×10^3 J/m^2.[44] At higher fluences direct experimental evidence for a bimodal distribution was obtained from high resolution Raman experiments.[25]

The fluence dependence in Fig. 9 shows that the ratio of the anti-Stokes signals obtained for the 0.5 and 15 ns pulses decreases as the fluence increases. This observation, which is in agreement with the photoacoustic results,[43] shows that in the low fluence range intensity plays a more important role in the infrared multiphoton excitation of SF_6 than in the high fluence range. At low excitation high intensity is needed to over-come the anharmonic shift of the energy levels.[45] In this regime the fraction of molecules excited high enough to show a change in Raman spectrum depends more on intensity than it does the in high fluence range. Once the molecules are excited to a regime where the many intramolecular couplings help excitation, only fluence plays a role. Therefore the increase in anti-Stokes signal, which is a direct consequence of intramolecular couplings, depends also somewhat on intensity in the low fluence regime.

In Fig. 11 the dependence of the anti-Stokes signals on the infrared pumping wavelength is shown for both 15 ns and 0.5 ns multiphoton excitation. Because of the anharmonic shift of the levels at high excitation, the signals shift toward the red by about 5 cm^{-1} from the center of the one photon absorption band. The present data matches the absorption profiles for SF_6 at a temperature of 450 K,[46] much lower than the 2800 K final temperature corresponding to the average absorption of 25 infrared photons per molecule at 10^4 J/m^2. The width of the multiphoton excitation profiles also shows some intensity broadening.

The results shown in Fig. 11 agree with the infrared multiphoton absorption profile[47] and the frequency dependence of the infrared multiphoton dissociation probability[48] for SF_6 reported in the literature. This implies that the anti-Stokes Raman signal is proportional to the total vibrational energy stored in the molecule for all the CO_2-lines within the absorption profile, and not only for the center frequency. Therefore a rapid intramolecular vibrational energy equilibrium appears to be established for collisionless infrared multiphoton excitation at all frequencies that lie within the absorption profile of SF_6.

VI. CONCLUSIONS

This paper presents detailed measurements on collisionless infrared multiphoton excited SF_6. Spontaneous Raman spectroscopy is used as a tool to monitor the energy in the strong Raman active ν_1-mode. The pressure dependence of the observed signals clearly proves that one is dealing with a

collisionless process. Furthermore, the results present strong evidence that an intramolecular equilibrium among the various vibrational modes is achieved within the 20 ns time-resolution of the experiment.

We have observed a red shift and intensity broadening of the pump-frequency dependence and determined the fluence dependence of the increase in Raman signal. The observations are in excellent agreement with the results obtained by other techniques, such as dissociation and photoacoustic measurements. These techniques, however, monitor the total vibrational energy in the molecules, whereas the present experimental technique is only sensitive to the energy in one single mode.

For SF_6 in the gas phase, one is limited to probing one single Raman active mode. Experiments on molecules that have more than one accessible Raman active mode are in progress. These experiments should provide further information on the intramolecular energy distribution in collisionless infrared multiphoton excited molecules. Even more detail will be provided by forthcoming picosecond coherent anti-Stokes Raman spectroscopy experiments on infrared multiphoton excited molecules.

ACKNOWLEDGMENTS

The authors gratefully acknowledge helpful comments and stimulating discussions with Prof. N. Bloembergen. This research was supported by the U.S. Army Research Office and the Joint Services Electronics Program under contracts no. DAAG29-85-K-0600 and N00014-84-K-0465, respectively, with Harvard University.

[1]N. R. Isenor, V. Merchant, R. S. Hallsworth, and M. C. Richardson, Can. J. Phys. **51**, 1281 (1973).

[2]See, e.g, the following publications and references therein. V. N. Bagratashvili, V. S. Letokhov, A. A. Makarov, and E. A. Ryabov, *Multiple Photon Infrared Laser Photophysics and Photochemistry* (Harwood Academic, New York, 1985); N. Bloembergen and E. Yablonovitch, Phys. Today **5**, 23 (1978); W. Fuss and K. L. Kompa, Prog. Quantum Electron. **7**, 117 (1981); D. S. King, *Dynamics of the Excited State,* edited by K. P. Lawley (Wiley, New York, 1982).

[3]R. V. Ambartsumian, V. S. Letokhov, E. A. Ryabov, and N. V. Chekalin, JETP Lett. **20**, 273 (1974).

[4]V. S. Letokhov, Phys. Today **5**, 25 (1977).

[5]M. Drouin, M. Gauthier, R. Pilon, P. A. Hackett, and C. Willis, Chem. Phys. Lett. **60**, 16 (1978).

[6]J. B. Marling and I. P. Herman, J. Chem. Phys. **72**, 5603 (1980).

[7]Aa. S. Sudbø, P. A. Schulz, E. R. Grant, Y. R. Shen, and Y. T. Lee, J. Chem. Phys. **68**, 1306 (1978); **70**, 912 (1979).

[8]C. R. Quick, Jr. and C. Wittig, J. Chem. Phys. **72**, 1694 (1980).

[9]V. N. Bagratashvili, M. V. Kuzmin, and V. S. Letokhov, J. Chem. Phys. **88**, 5780 (1984).

[10]M. Quack, J. Chem. Phys. **69**, 1282 (1978).

[11]C. D. Cantrell, S. M. Freund, and J. L. Lyman, *Laser Handbook,* edited by M. L. Stitch (North-Holland, Amsterdam, 1979), Vol. 3.

[12]S. Mukamel, Adv. Chem. Phys. **47**, 509 (1981).

[13]J. R. Ackerhalt, H. W. Galbraith, and P. W. Milonni, Phys. Rev. Lett. **51**, 1259 (1983).

[14]G. Hose and H. S. Taylor, Chem. Phys. **84**, 375 (1984); G. Hose, H. S. Taylor, and Y. Bai, J. Chem. Phys. **80**, 4363 (1984).

[15]I. Schek and R. E. Wyatt, J. Chem. Phys. **83**, 4650 (1985).

[16]N. Bloembergen and A. H. Zewail, J. Phys. Chem. **88**, 5459 (1984).

[17]N. Bloembergen and E. Yablonovitch, Phys. Today **5**, 23 (1978).

[18]H. W. Galbraith and J. R. Ackerhalt, in *Laser Induced Chemical Processes,* edited by J. I. Steinfeld (Plenum, New York, 1981).

[19]D. W. Noid, M. L. Koszykowski and R. A. Marcus, Annu. Rev. Phys. Chem. **32**, 267 (1981).

[20]P. M. Felker and A. H. Zewail, Chem. Phys. Lett. **102**, 113 (1983); **108**, 303 (1984); see also, Phys. Rev. Lett. **53**, 501 (1984).

[21]P. Mazur and E. W. Montroll, J. Math. Phys. **1**, 70 (1960).

[22]V. N. Bagratashvili, Yu. G. Vainer, V. S. Doljikov, S. F. Koliakov, A. A. Makarov, L. P. Malyavkin, E. A. Ryabov, E. G. Silkis, and V. D. Titov, Appl. Phys. **22**, 101 (1980).

[23]V. N. Bagratashvili, Yu. G. Vainer, V. S. Dolzhikov, S. F. Kol'yakov, V. S Letokhov, A. A. Makarov, L. P. Malyavkin, E. A. Ryabov, E. G. Sil'kis, and V. D. Titov, Sov. Phys.—JETP **53**, 512 (1981).

[24]V. N. Bagratashvili, V. S. Doljikov, V. S. Letokhov, A. A. Makarov, L. P. Maljavkin, E. A. Ryabov, E. G. Silkis, and Yu. G. Vainer, Opt. Commun. **38**, 31 (1981).

[25]V. N. Bagratashvili, Yu. G. Vainer, V. S. Doljikov, V. S. Letokhov, A. A. Makarov, L. P. Malyavkin, E. A. Ryabov, and E. G. Sil'kis, Opt. Lett. **6**, 148 (1981).

[26]Yu. S. Doljikov, V. S. Letokhov, A. A. Makarov, A. L. Malinovsky, and E. A. Ryabov, Chem. Phys. Lett. **124**, 304 (1986).

[27]V. S. Doljikov, Yu. S. Doljikov, V. S. Letokhov, A. A. Makarov, A. L. Malinovsky, and E. A. Ryabov, Chem. Phys. **102**, 155 (1986).

[28]D. S. Frankel and T. J. Manuccia, Chem. Phys. Lett. **54**, 451 (1978).

[29]R. C. Sharp, E. Yablonovitch, and N. Bloembergen, J. Chem. Phys. **74**, 5357 (1981).

[30]P. Mukherjee and H. S. Kwok, J. Chem. Phys. **84**, 1285 (1986).

[31]E. Mazur, I. Burak, and N. Bloembergen, Chem. Phys. Lett. **105**, 258 (1984).

[32]G. Placzek, *Marx Handbuch der Radiologie,* 2nd ed. (Academische Verlagsgesellschaft, Leipzig, 1934), Vol. VI, p. 206.

[33]Eric Mazur, Rev. Sci. Instrum. **57**, 2507 (1986).

[34]A. Gondhalekar, N. R. Heckenberg, and E. Holzhauer, IEEE J. Quantum Electron. **QE-11**, 103 (1975).

[35]H. S. Kwok and E. Yablonovitch, Appl. Phys. Lett. **27**, 583 (1975).

[36]H. S. Kwok and E. Yablonovitch, Opt. Commun. **21**, 252 (1977).

[37]E. Yablonovitch and J. Goldhar, Appl. Phys. Lett. **25**, 580 (1974).

[38]G. Herzberg, *Molecular Spectra and Molecular Structure* (Reinhold, New York, 1979), Vol. 2.

[39]See, e.g, W. Feller, *An Introduction to Probability Theory and Its Applications* (Wiley, New York, 1971).

[40]R. D. Bates, Jr., J. T. Knudtson, G. W. Flynn, and A. M. Ronn, Chem. Phys. Lett. **8**, 103 (1971).

[41]J. I. Steinfeld, I. Burak, D. G. Sutton, and A. V. Nowak, J. Chem. Phys. **52**, 5421 (1970).

[42]W. Fuss and J. Hartmann, J. Chem. Phys. **70**, 5468 (1979).

[43]J. G. Black, P. Kolodner, M. J. Schultz, E. Yablonovitch, and N. Bloembergen, Phys. Rev. A **19**, 704 (1979).

[44]V. M. Apatin, V. M. Krivtsun, Yu. A. Kuritsyn, G. N. Makarov, and I. Pak, Opt. Commun. **47**, 251 (1983).

[45]T. B. Simpson, J. G. Black, I. Burak, E. Yablonovitch, and N. Bloembergen, J. Chem. Phys. **83**, 628 (1985).

[46]A. V. Nowak and J. L. Lyman, J. Quant. Spectrosc. Radiat. Transfer **15**, 945 (1975).

[47]D. O. Ham and M. Rothschild, Opt. Lett. **1**, 28 (1977).

[48]F. Brunner, T. P. Cotter, K. L. Kompa, and D. Proch, J. Chem. Phys. **67**, 1547 (1977); F. Brunner and D. Proch, J. Chem. Phys. **68**, 4936 (1978).

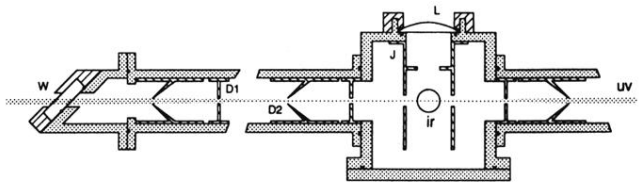

FIG. 2. Cross-sectional view of the Raman cell. W = quartz window, D1, D2 = straight and conical baffles, J = stray light jacket, IR = position of ir pump beam, UV = probing uv beam, L = collimating lens. The window holder has been rotated by 90° to show the Brewster angle mounting.